

JWST observations of K2-18b can be explained by a gas-rich mini-Neptune with no habitable surface

NICHOLAS F. WOGAN,^{1,2} NATASHA E. BATALHA,¹ KEVIN ZAHNLE,^{1,2} JOSHUA KRISSANSEN-TOTTON,^{3,2} SHANG-MIN TSAI,⁴
AND RENYU HU^{5,6}

¹*Space Science Division, NASA Ames Research Center, Moffett Field, CA 94035*

²*Virtual Planetary Laboratory, University of Washington, Seattle, WA 98195*

³*Department of Earth and Space Sciences, University of Washington, Seattle, WA 98195*

⁴*University of California Riverside, Riverside, CA 92521*

⁵*Jet Propulsion Laboratory, California Institute of Technology, Pasadena, CA 91109*

⁶*Division of Geological and Planetary Sciences, California Institute of Technology, Pasadena, CA 91125*

ABSTRACT

JWST recently measured the transmission spectrum of K2-18b, a habitable-zone sub-Neptune exoplanet, detecting CH₄ and CO₂ in its atmosphere. The discovery paper argued the data are best explained by a habitable “Hycean” world, consisting of a relatively thin H₂-dominated atmosphere overlying a liquid water ocean. Here, we use photochemical and climate models to simulate K2-18b as both a Hycean planet and a gas-rich mini-Neptune with no defined surface. We find that a lifeless Hycean world is hard to reconcile with the JWST observations because photochemistry only supports < 1 part-per-million CH₄ in such an atmosphere while the data suggest about ~ 1% of the gas is present. Sustaining %-level CH₄ on a Hycean K2-18b may require the presence of a methane-producing biosphere, similar to microbial life on Earth ~ 3 billion years ago. On the other hand, we predict that a gas-rich mini-Neptune with 100× solar metallicity should have 4% CH₄ and nearly 0.1% CO₂, which are compatible with the JWST data. The CH₄ and CO₂ are produced thermochemically in the deep atmosphere and mixed upward to the low pressures sensitive to transmission spectroscopy. The model predicts H₂O, NH₃ and CO abundances broadly consistent with the non-detections. Given the additional obstacles to maintaining a stable temperate climate on Hycean worlds due to H₂ escape and potential supercriticality at depth, we favor the mini-Neptune interpretation because of its relative simplicity and because it does not need a biosphere or other unknown source of methane to explain the data.

1. INTRODUCTION

Whether or not life is abundant in the galaxy depends on the frequency of habitable worlds. The Kepler era of exoplanet exploration revealed that close-in sub-Neptunes (~ 2.4 R_⊕) have high occurrence rates (Fulton & Petigura 2018). These planets have bulk densities that can be explained by several planetary models that range from a massive H₂ atmosphere similar to Neptune’s, to a thin hydrogen atmosphere (e.g., ~ 1 bar) overlying a H₂O-rich interior. Researchers have suggested that H₂O-rich sub-Neptunes could have habitable surface oceans provided that the climate is suitable for liquid water (Madhusudhan et al. 2021). These so-called “Hycean” worlds, if they exist, have the potential to be among the most common habitable planetary environments.

Perhaps the best known Hycean world candidate is the sub-Neptune K2-18b (8.63 M_⊕, 2.61 R_⊕; Benneke et al. 2019), which was recently observed by the James Webb Space Telescope (i.e., JWST; Madhusudhan et al. 2023b). The transmission spectrum reveals strong evidence for CH₄ and CO₂ in a H₂-rich atmosphere. Furthermore, JWST did not detect NH₃, H₂O or CO. Madhusudhan et al. (2023b) argued the data are best explained by a habitable Hycean world because, according to past photochemical studies, such a planet can be consistent with the NH₃ non-detection (Tsai et al. 2021a; Yu et al. 2021; Madhusudhan et al. 2023a; Hu et al. 2021). Ammonia is instead expected on a mini-Neptune with a massive hydrogen atmosphere (e.g., Yu et al. 2021; Hu et al. 2021). Furthermore, Madhusudhan et al. (2023b) favored a Hycean world because their retrieved ~ 1% abundances for CH₄ and CO₂ are broadly compatible with photochemical modeling predictions made by Hu et al. (2021) for a Hycean K2-18b.

Here, we use 1-D photochemical and climate models to revisit the past calculations (Hu et al. 2021; Yu et al. 2021; Tsai et al. 2021a) that support a habitable ocean-world interpretation of the data. We simulate K2-18b as a

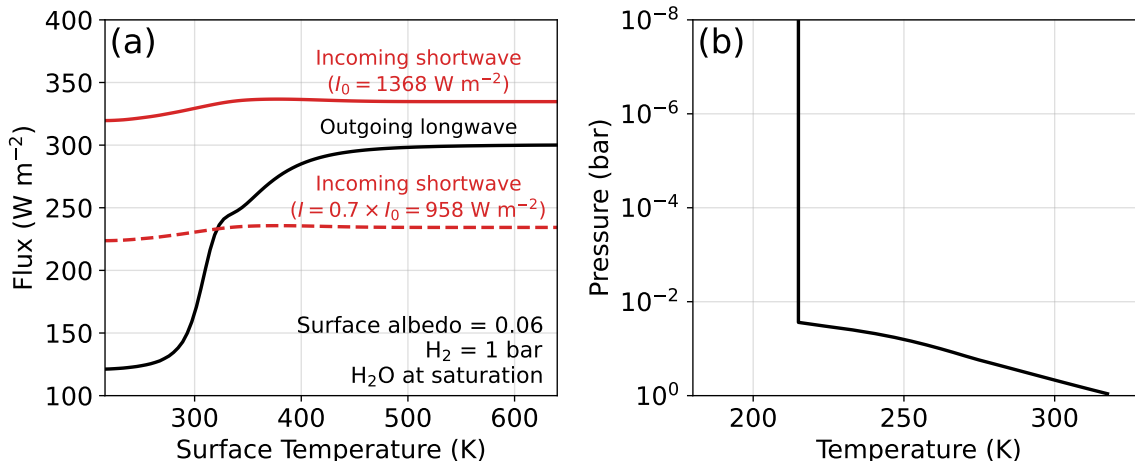


Figure 1. The climate of a plausible Hycean K2-18b. (a) shows the incoming shortwave (red) and outgoing longwave radiation (black) as a function of surface temperature computed with the climate model in *Photochem*. Calculations assume 1 bar of H_2 with H_2O at saturation in the troposphere. The solid red line is the incoming shortwave radiation for K2-18b’s full stellar insolation (1368 W m^{-2}), which can not be balanced by outgoing longwave energy below the critical point of H_2O ($< 647 \text{ K}$). The dashed red line considers a 30% smaller insolation to crudely represent high-altitude clouds reflecting away starlight, which would allow for a stable $\sim 320 \text{ K}$ climate. (b) the P-T profile for the stable climate in (a) which we adopt for the Hycean photochemical simulations.

Hycean planet to determine whether the CH_4 and CO_2 suggested by JWST are photochemically stable in such an atmosphere. Our Hycean models consider both a lifeless and inhabited planet, the latter represented by a primitive microbial biosphere that influence atmosphere chemistry. We also model K2-18b as a gas-rich mini-Neptune with a deep atmosphere. By comparing our simulations to the JWST data, and considering the relative complexities for each simulated composition, we suggest the most likely planetary model for K2-18b.

2. METHODS

2.1. Hycean worlds

To simulate a Hycean K2-18b, we first modeled a pressure-temperature (P-T) profile using the climate code contained within the *Photochem* software package (Wogan et al. 2023). The climate model uses correlated-k radiative transfer with opacities detailed in Appendix D of Wogan et al. (2023). The code constructs P-T profiles assuming the lower atmosphere follows a moist-pseudo adiabat connected to an isothermal stratosphere. For K2-18b, we assume a 215 K stratosphere following Hu (2021). Our approach can consider any number of condensing species (e.g., Graham et al. 2021), but H_2O is the most important condensable for a habitable K2-18b.

For a Hycean K2-18b, we nominally assume a 1-bar H_2 -dominated atmosphere with a water-saturated troposphere to facilitate comparison with previous work (Hu et al. 2021; Madhusudhan et al. 2023a; Innes et al. 2023). For such a composition, our cloud-free climate model predicts that K2-18b would not be habitable because the surface temperature would exceed the critical point of H_2O (Figure 1a), consistent with past studies (Innes et al. 2023; Scheucher et al. 2020). However, it has been suggested that high-altitude clouds or hazes could potentially reflect short wave radiation allowing for a cooler climate (Madhusudhan et al. 2021; Piette & Madhusudhan 2020). To approximate the cooling effects of clouds in our cloud-free climate simulations, following Hu et al. (2021), we arbitrarily reduce the incoming solar radiation by 30% which permits a $\sim 320 \text{ K}$ surface (Figure 1a). We adopt this habitable P-T profile, shown in Figure 1b, for all Hycean scenarios. Our photochemical simulations include up to %-level CH_4 and CO_2 , but the Figure 1b P-T profile ignores their greenhouse contribution. For this analysis, this is justified because the climate of a Hycean K2-18b is uncertain, and our climate model predicts the surface temperature would increase by $\lesssim 10 \text{ K}$ when accounting for CH_4 and CO_2 .

With our estimated P-T profile (Figure 1b), we then simulate steady-state photochemistry using *Photochem* (Wogan 2024a). The photochemical model contained in *Photochem* solves a system of partial differential equations approximating molecular transport in the vertical direction and the effect of chemical reactions, photolysis and condensation. We have made several updates to the reaction network and thermodynamic data originally published in Wogan et al.

Table 1. Model scenarios

Model type	Model #	K_{zz} ^a	Metallicity	Lower boundary condition ^d			
				N ₂	CO ₂	CH ₄	CO
Lifeless Hycean ^b	1	5×10^5	-	$f = 3 \times 10^{-3}$	$f = 8 \times 10^{-3}$	$\Phi = 0$	$\Phi = 0$
Inhabited Hycean ^b	2	5×10^5	-	$f = 3 \times 10^{-3}$	$f = 8 \times 10^{-3}$	$\Phi = 5 \times 10^{10}$	$v_d = 1.2 \times 10^{-4}$
Mini-Neptune ^c	3	Figure A1b	100× solar	$f = \text{chemical equilibrium}^e$			

^aThe vertically-constant eddy diffusion coefficient in $\text{cm}^2 \text{s}^{-1}$

^bAll Hycean models include $7 \times 10^{-3} \text{ cm s}^{-1}$ deposition velocities for HCN and HCCCN (Wogan et al. 2023), and impose a $10^{-5} \text{ cm s}^{-1}$ deposition velocity for C₂H₆ (Hu et al. 2021).

^cThe mini-Neptune case has a solar C/O ratio and a 60 K intrinsic temperature.

^dThe variable f indicates a fixed lower-boundary mixing ratio, Φ indicates a fixed surface flux in molecules $\text{cm}^{-2} \text{s}^{-1}$, and v_d indicates a surface deposition velocity in cm s^{-1} . If a fixed surface flux is specified, then the deposition velocity is zero. In Hycean simulations, unspecified molecules have a zero-flux lower boundary condition.

^eIn the mini-Neptune case, we assume fixed lower boundary conditions at chemical equilibrium for molecules with equilibrium concentrations $> 10^{-8}$ mixing ratio. For lower concentration molecules, we permit molecules to mix into the deep atmosphere (> 500 bar) with a deposition velocity $v_d = K_{zz}/H$, where H is scale height, following past works (Moses et al. 2000).

(2023). We improved the kinetics and thermodynamics of CH₃O, H₂COH and related species, all of which are detailed in Appendix Table A1. For key reactions, we nominally adopt new kinetics following Xu et al. (2015), but we also consider alternative rates from Klippenstein (2023). These updates are important for estimating photochemical methane production on Hycean worlds as discussed in Section 3.1. We have also updated our H₂O and H₂ photolysis data (Appendix Table A1). The updated network is available on Zenodo (see the “.yaml” files in the “input/” folder of Wogan (2024b)). Because the UV spectrum of K2-18 has not been measured, we instead use the UV spectrum of GJ 176 measured by the MUSCLES survey for our photochemical calculations (France et al. 2016) following the Hu et al. (2021) analysis.

2.2. Mini-Neptune world

We additionally model K2-18b as a gas-giant mini-Neptune with no habitable surface. We take the same approach as Hu (2021) and simulate the massive hydrogen atmosphere over two stages: The first considers the deep atmosphere (500 to 1 bar), and the second simulates the upper atmosphere (1 to 10^{-8} bar). The lower atmosphere stage captures the equilibrium-to-disequilibrium transition (i.e., gas quenching) that occurs deep in a gas-giant atmosphere (e.g., Zahnle et al. 2016), while the upper atmosphere model approximates the impact of UV photolysis and gas condensation on composition.

For the first stage, we use the *PICASO* climate model (Mukherjee et al. 2023) to generate a P-T profile with opacities appropriate for a 100× solar metallicity with a solar C/O at chemical equilibrium assuming a geothermal heat flow consistent with an intrinsic temperature (T_{int}) of 60 K (Hu 2021). Note that the intrinsic temperature affects the upper atmosphere abundance of gases such as CH₄ (Fortney et al. 2020). We discuss this T_{int} dependence in Section 3.2, but leave a full parameter space exploration for future work. Next, using the P-T profile, we do a full kinetics simulation with the *Photochem* model between 500 bar and 1 bar using our network of ~ 600 reversible reactions described previously (Section 2.1). We fix the lower boundary to chemical equilibrium composition, and allow the kinetics model to predict the chemical equilibrium-to-disequilibrium transition. The deep atmosphere adopts an altitude-independent eddy diffusion coefficient of $K_{zz} = 10^8 \text{ cm}^2 \text{ s}^{-1}$ following Hu (2021).

In the second stage we simulate K2-18b’s upper atmosphere using results from the first stage as lower boundary conditions. We do not use the *PICASO* P-T profile above 1 bar because *PICASO* assumes the entire atmospheric profile is at chemical equilibrium which would not be the case for the cool upper atmosphere of K2-18b. The chemical equilibrium assumption creates a stratospheric inversion in the P-T profile from greenhouse gases such as CH₄. Furthermore, *PICASO* assumes a dry convective lapse rate but the P-T profile in much of the upper troposphere should follow a moist-pseudo adiabat because of water condensation. As an alternative to *PICASO*, we extrapolate the P-T profile above the 1 bar level by drawing an adiabat upwards using the *Photochem* climate model until it intersects an

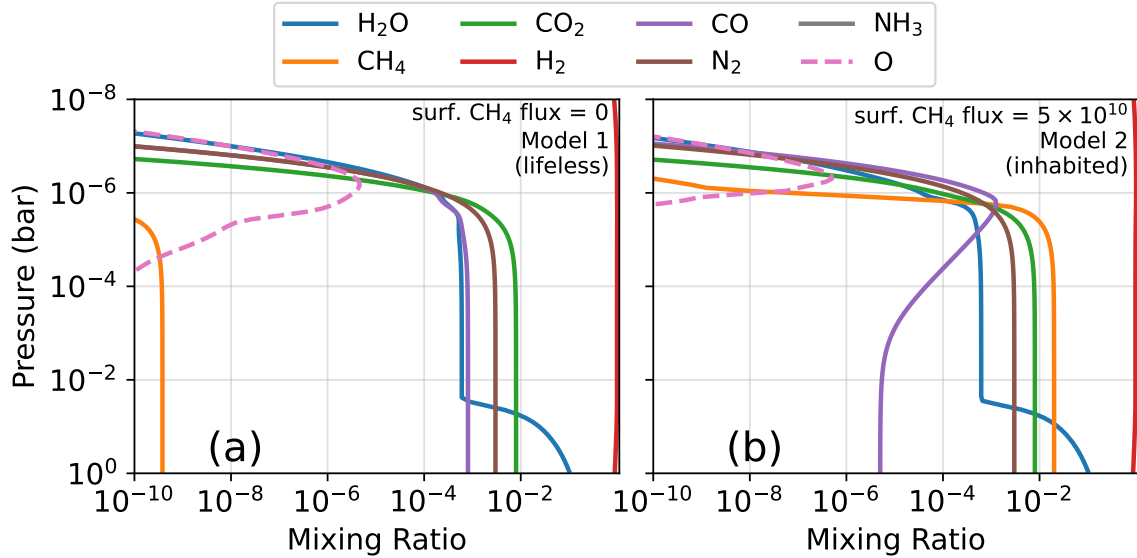


Figure 2. Photochemical simulations of K2-18b as a habitable Hycean world. Panels (a) and (b) correspond to Model 1 and 2, respectively, described in Table 1. Both panels include the surface CH_4 flux in molecules $\text{cm}^{-2} \text{s}^{-1}$ required to sustain the CH_4 concentration. (a) shows that only ppb-level methane can accumulate photochemically (i.e., abiotically). (b) shows that methane is predicted to build-up to %-levels assuming a biological surface CH_4 flux of 5×10^{10} molecules $\text{cm}^{-2} \text{s}^{-1}$ which is about half of the modern Earth’s biological flux (Jackson et al. 2020).

isothermal 215 K stratosphere. Appendix Figure A1a compares the *PICASO* profile to the modified profile that we adopt. Finally, using the modified P-T profile, we compute the photochemical steady-state of the upper atmosphere (1 to 10^{-8} bar) to predict its composition. At the lower boundary, we fix all gas concentrations to the values predicted at the 1 bar level of the lower atmosphere kinetics simulation described in the previous paragraph. The upper atmosphere simulation assumes a Jupiter-like eddy diffusion profile as used in Hu (2021) (Appendix Figure A1b).

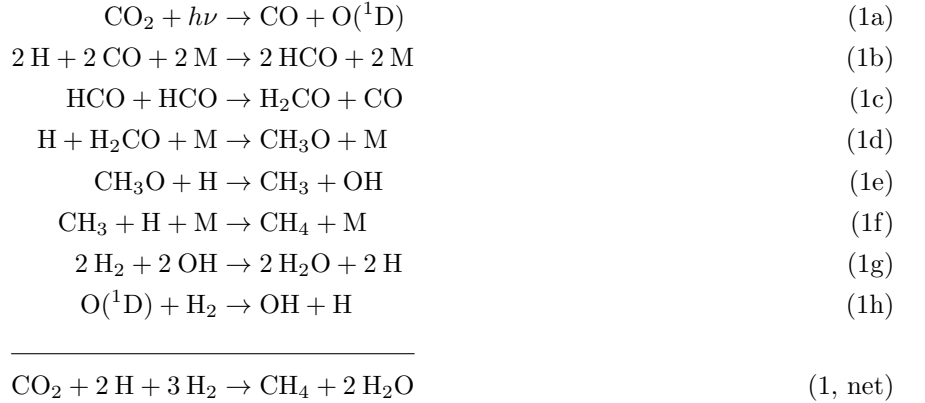
2.3. Transmission spectra

We use the *PICASO* code (Batalha et al. 2019) to compute the transmission spectra of simulated Hycean and mini-Neptune atmospheres adopting the $R=60,000$ resampled opacities archived on Zenodo (Batalha et al. 2022). The main text presents clear-sky spectra because the JWST data do not favor high altitude clouds. The Appendix shows the spectral effects of water, elemental sulfur (S_2 and S_8) and hydrocarbon clouds and hazes.

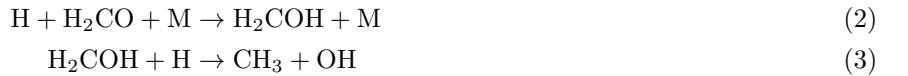
3. RESULTS

3.1. Hycean worlds

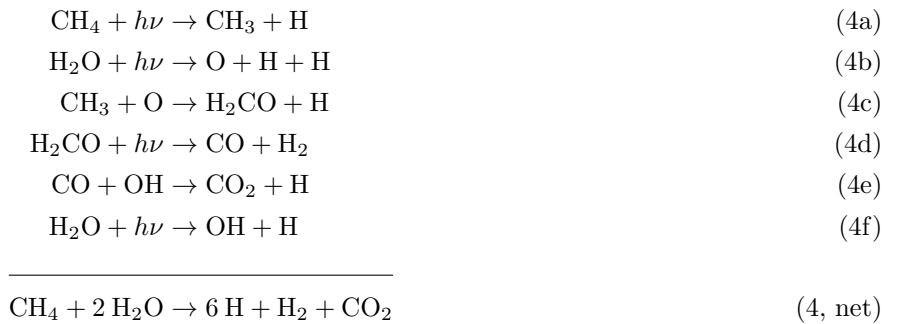
To investigate K2-18b as a Hycean world we first consider an uninhabited planet. Our nominal simulation, called “model 1”, assumes a 1 bar H_2 -dominated atmosphere, 0.8% CO_2 fixed at the surface, and other settings and boundary conditions detailed in Table 1. We choose 0.8% CO_2 because it is the median concentration implied by the JWST spectrum (Madhusudhan et al. 2023b). Methane has a zero-flux lower boundary condition, therefore all accumulated CH_4 is the result of the photochemical reduction of CO_2 to CH_4 . Figure 2a shows the steady-state composition of the model 1 atmosphere as a function of pressure revealing that only 0.4 part-per-billion (ppb) CH_4 is photochemically stable. Methane is slowly produced by the following sequence of reactions:



By analyzing column-integrated reaction rates we have determined that Reaction (1d) is the rate-limiting step. Another important path with the same net reaction replaces both reactions involving CH₃O with alternatives that depend on the isomer H₂COH:



Methane is effectively destroyed by photolysis followed by several oxidizing reactions:



In H₂-rich solar system atmospheres (e.g., Saturn’s), methane has a long lifetime to destruction because, after photolysis (Reaction (4a)), it recombines: CH₃ + H + M → CH₄ + M (Moses et al. 2000). The same recombination is inefficient in model 1 because, unlike the gas-giants in the solar system, model 1 has substantially more oxidizing gases like H₂O. In particular, water vapor photolysis at Ly-α wavelengths (λ = 126.56 nm) produces oxygen atoms (Reaction (4b), Slanger & Black 1982) that rapidly oxidize CH₃ before CH₄ is reformed. Methyl is also destroyed by atomic oxygen sourced from a sequence of reactions involving CO₂ photolysis: CO₂ + hν → CO + O, H₂O + hν → H + OH, and CO + OH → CO₂ + H which has the net reaction H₂O + hν → O + H + H. Overall, efficient methyl oxidation in addition to slow CH₄ production (Reaction path (1)), results in only trace amounts of atmospheric CH₄.

Our result that CH₄ cannot accumulate in model 1 is not sensitive to many model assumptions. For example, we have recomputed model 1 with vertically constant K_{zz} between 10⁴ and 10⁶ cm² s⁻¹, N₂ concentrations (f_{N_2}) between ~ 1 ppm and 1%, and troposphere relative humidities (ϕ) spanning 0.1 to 1. Within this parameter space, our photochemical code predicts the maximum stable CH₄ concentration is only 4 ppb for $K_{zz} = 10^4$ cm² s⁻¹, $f_{\text{N}_2} = 1$ ppm, and $\phi = 1$. As an additional test, we recomputed model 1 using alternative rates for Reactions 1d and 2 derived by Klippenstein (2023) using ab initio methods. Klippenstein (2023) predicts that these important rate-limiting reactions are faster than the Xu et al. (2015) rates we nominally assume (Appendix Table A1) at the temperatures and pressures relevant to Hycean atmospheres. Despite this difference, our model using the Klippenstein (2023) rates predicts only 32 ppb CH₄.

Up to this point, we have modeled K2-18b as a habitable, yet uninhabited planet. Now we consider an inhabited case, which we refer to as model 2. Model 1 imposes the surface concentration of H₂, CO₂ and N₂, but most all other gases, including CH₄ and CO, are dictated by photochemistry. If K2-18b is a Hycean world inhabited by microbial life then CH₄ and CO could be biologically modulated gases like they were on the anoxic Archean Earth (Kharecha

et al. 2005; Wogan & Catling 2020; Thompson et al. 2022). Chemosynthetic methanogens can consume H_2 and CO_2 for energy, producing methane as a waste gas:



CO is also food for acetogenic microbes:



The produced CH_3COOH could have been food for acetotrophic methanotrophs ($\text{CH}_3\text{COOH} \rightarrow \text{CH}_4 + \text{CO}_2$). Model 2 simulates K2-18b as a Hycean world with boundary conditions representing biological influence from these early Archean metabolisms (Table 1). To model methanogenic life, we impose a surface CH_4 flux needed to replicate the %-level concentration implied by the JWST data, which ended up being half the modern Earth’s biological methane flux (5×10^{10} molecules $\text{cm}^{-2} \text{s}^{-1}$, Jackson et al. 2020). We also add a CO deposition velocity of 1.2×10^{-4} cm s^{-1} to approximate the influence of CO-consuming acetogens (Reaction (6), Kharecha et al. 2005). At photochemical steady-state, model 2 has 2% CH_4 and a $\sim 10^{-5}$ CO mixing ratio at the surface (Figure 2b).

With a methanogenic biosphere, CH_4 can accumulate to the %-levels suggested by recent JWST observations (Madhusudhan et al. 2023b). In contrast, on an uninhabited Hycean K2-18b, CH_4 should be at only ppb-levels (model 1) because large concentrations can not accumulate photochemically and other non-biological sources of methane seem implausible (Section 4).

3.2. Mini-Neptune world

Figure 3 shows K2-18b modeled as a gas-giant mini-Neptune with no habitable surface (i.e., model 3 in Table 1). Deep in the atmosphere, at 500 bar and 1700 K, fast reactions enforce chemical equilibrium for our assumed composition of $100\times$ solar metallicity with a solar C/O ratio. As gases mix upward to lower pressures and temperatures, reactions slow, causing an equilibrium-to-disequilibrium transition (i.e., gas quenching). N_2 and NH_3 chemistry quenches near 200 bar and ~ 1400 K, and the CO_2 -CO- CH_4 system fails to maintain equilibrium near 100 bar and ~ 1250 K. These quench points are broadly consistent with Hu (2021) who constructed similar mini-Neptune models of K2-18b.

Quenched gases from the deep atmosphere mix upward to Model 3’s stratosphere where they are relevant to transmission spectroscopy. The atmosphere has 4% CH_4 along with 0.06% CO_2 at 1 mbar, which is broadly consistent with recent JWST observations (Madhusudhan et al. 2023b). Water vapor condensation between 0.07 bar and 4 mbar reduces its concentration, causing only 0.3% of the gas to be present at 1 mbar. At the same pressure level, there is also 0.3% CO and 0.07% NH_3 . Only trace photochemically produced SO_2 is present ($\sim 10^{-7}$ mixing ratio) as most all sulfur is photochemically processed to S_2 and S_8 in the lower atmosphere where it condenses out (Zahnle et al. 2016).

We additionally tested the sensitivity of Model 3 to the assumed intrinsic temperature ($T_{\text{int}} = 60$ K), as this parameter can impact deep atmosphere quenching and the resulting stratospheric abundances of CH_4 , CO_2 , and CO (Fortney et al. 2020; Tsai et al. 2021b). Larger T_{int} (e.g, 100 K) drives an increase in CO that is hard to reconcile with JWST observations. For lower T_{int} values (e.g., 30 K), our model does not produce enough CO_2 to explain the JWST data. Future abundance constraints from JWST offer an exciting avenue to study K2-18b’s internal temperature and thermal evolution. We leave detailed exploration of this topic to a future study.

3.3. Transmission spectra and comparison to JWST data

Figure 4 shows the simulated clear-sky transmission spectra of three scenarios for K2-18b compared to JWST NIRISS and NIRSpec observations: A lifeless Hycean planet (model 1), a Hycean world inhabited by an Archean-like biosphere (model 2) and a $100\times$ solar metallicity mini-Neptune with no habitable surface (Model 3). In all cases, we allow the simulated spectra to have an offset between the NIRISS and NIRSpec data as to best fit the observations, motivated by Madhusudhan et al. (2023b).

JWST data rules out model 1 ($\chi_r^2 = 3.22$) because the lifeless Hycean world does not have enough methane (~ 0.8 ppb, Figure 2) to explain the observed CH_4 absorption shortwards of $4 \mu\text{m}$. On the other hand, the data do not strongly exclude an inhabited Hycean world (model 2, $\chi_r^2 = 1.51$). Model 2 fits the CH_4 and CO_2 spectral features in the data because it has 2% of biologically-produced methane along with 0.8% CO_2 .

However, an inhabited Hycean world is not required to explain the data. Our model of a gas-giant mini-Neptune (model 3) has a comparable fit ($\chi_r^2 = 1.51$) largely because of its 4% CH_4 and 0.06% CO_2 at ~ 1 mbar. The spectra

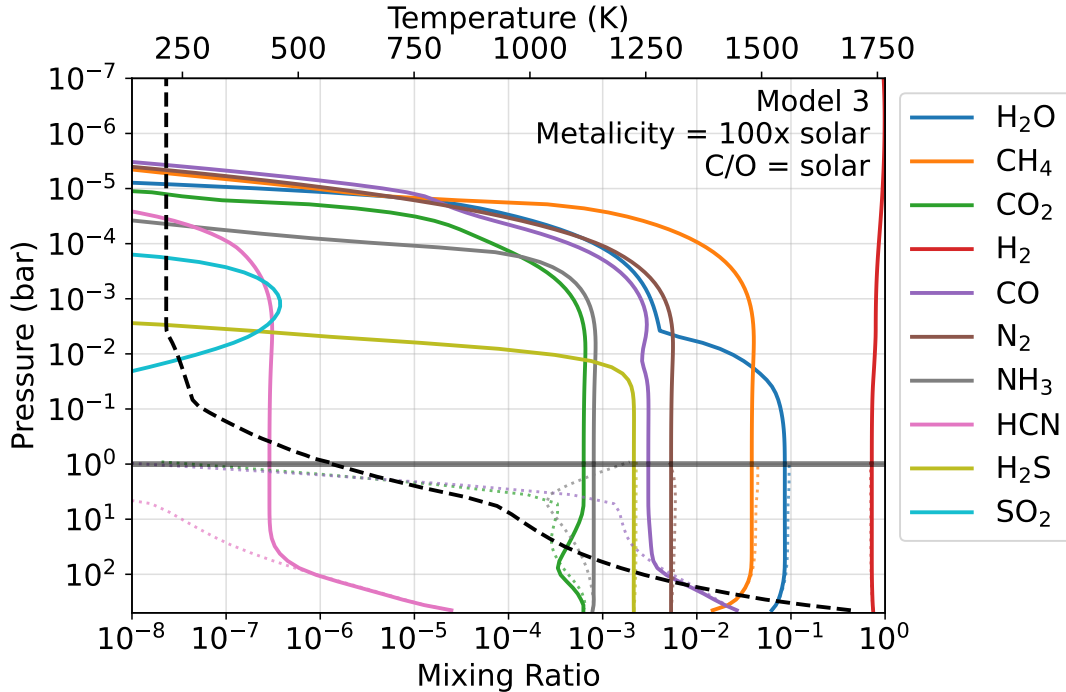


Figure 3. Climate and photochemical simulation of K2-18b as a mini-Neptune with no habitable surface (Model 3 in Table 1). The black dashed line is the computed P-T profile which is referenced to the upper x-axis. The horizontal grey line at 1 bar divides the lower and upper atmosphere as discussed in Section 2.1. Solid colored lines are predicted atmospheric composition from our photochemical model. For comparison, the dotted lines in the lower atmosphere are chemical equilibrium composition. If K2-18b is a $100\times$ solar mini-Neptune with a solar C/O ratio, then we predict the observable upper atmosphere should have $\sim 4\%$ CH_4 and nearly 0.1% CO_2 , which is in reasonable agreement with recent JWST observations (Madhusudhan et al. 2023b).

show small H_2O absorption because water vapor is cold trapped at ~ 4 mbar (Figure 3). Also, NH_3 has small absorption features at 1.5 , 2 , and $3 \mu\text{m}$. Madhusudhan et al. (2023b) used the JWST data to argue for an NH_3 upper bound of $\sim 3 \times 10^{-5}$ at 95% confidence assuming a vertically constant NH_3 concentration. At 1 mbar, our mini-Neptune model has 7×10^{-4} NH_3 , but photolysis rapidly diminishes the gas’s concentration towards lower pressures (see Figure 3). Using a transmission contribution function (Equation 8 in Mollière et al. (2019)) we find that the $3 \mu\text{m}$ NH_3 feature (Figure 4c) is sensitive to pressures between $\sim 10^{-3}$ and $\sim 10^{-5}$ bar where the ammonia concentration is between 7×10^{-4} and 10^{-14} mixing ratio. While a direct comparison is challenging, our modeled heterogeneous NH_3 profile appears broadly compatible with the vertically constant upper bound derived by Madhusudhan et al. (2023b).

Models 2 and 3, and the retrievals presented in Madhusudhan et al. (2023b), are not able to reproduce the apparent large absorption feature near $\sim 1 \mu\text{m}$ (red points in Appendix Figure A2). Disregarding these six data points reduces χ_r^2 values for both model 2 and 3 to about 1. Future visits with NIRISS SOSS will be valuable to determine whether the scatter near $\sim 1 \mu\text{m}$ is physical or instrumental.

Our conclusion that the data strongly rule out model 1 but not model 2 or 3 is unchanged when including various aerosol opacities (Appendix Figure A2). Accounting for aerosols, the model 1 simulated spectrum remains a poor fit ($\chi_r^2 = 2.33$) when compared to model 2 and 3 ($\chi_r^2 \approx 1.4$).

4. DISCUSSION

4.1. Reconciling our lifeless Hycean model with past research

Hu et al. (2021) pioneered the use of photochemical models to simulate K2-18b as a lifeless Hycean planet. They consider a 1 bar H_2 atmosphere, 1% N_2 , a comparable P-T profile to ours (Figure 1b), and CO_2 concentrations between 400 ppm and 10%. In all scenarios, they predict the photochemical accumulation of %-levels CH_4 , which contrasts with the ppb-level CH_4 we compute in very similar scenarios (e.g., model 1). There are two reasons our results differ. First, Hu et al. (2021) assumed that the photolysis of H_2O produces only $\text{OH} + \text{H}$. However, we demonstrate here that the seemingly minor channel that produces $\text{O} + \text{H} + \text{H}$ (Reaction 4b) is important for CH_4 destruction in K2-18b’s

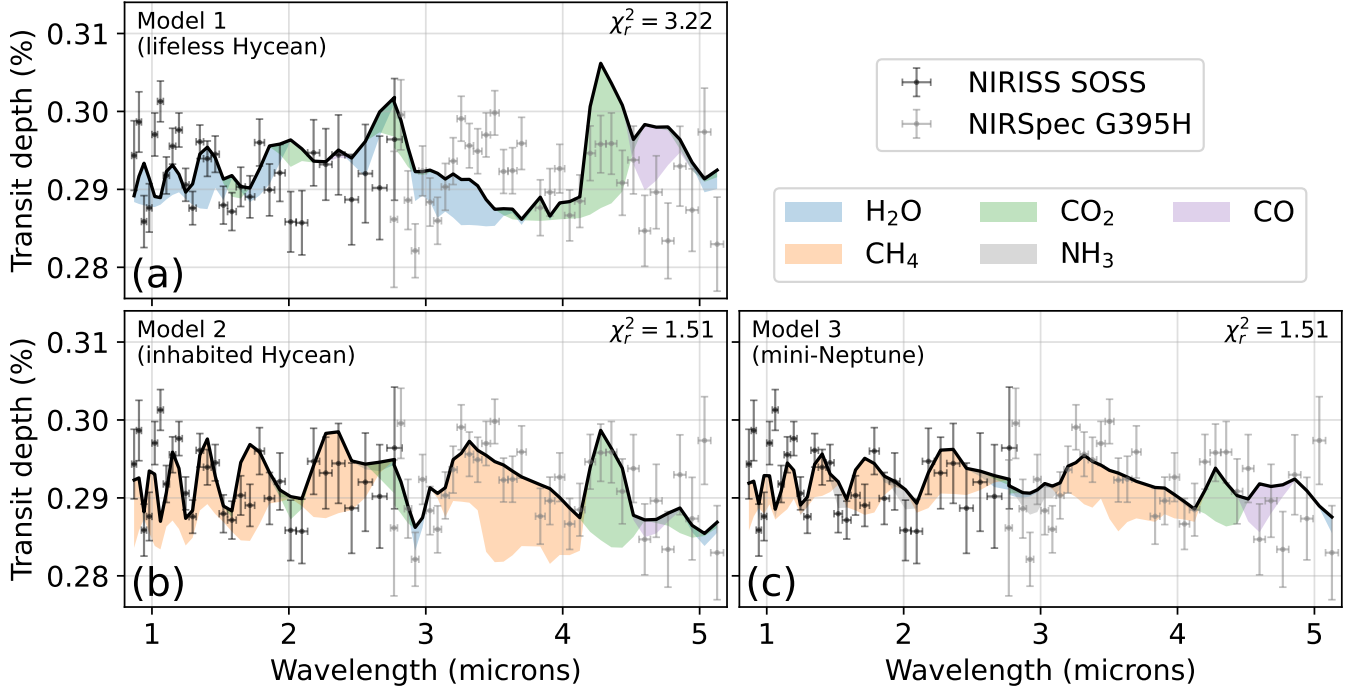


Figure 4. Transmission spectra of Hycean and mini-Neptune models of K2-18b compared to JWST NIRISS and NIRSPEC data from Figure 3 in [Madhusudhan et al. \(2023b\)](#). Panels (a), (b) and (c) show simulated clear-sky transmission spectra of models 1, 2 and 3, respectively. Colored shading shows the effect of molecules on the spectrum. The reported χ_r^2 values each have 64 degrees of freedom. The JWST data strongly rules out a lifeless Hycean world (model 1, $\chi_r^2 = 3.22$), but allows for either an inhabited Hycean (model 2) or mini-Neptune (model 3) model of K2-18b ($\chi_r^2 = 1.51$).

atmosphere. To verify this insight, we have rerun the 400 ppm- CO_2 model of [Hu et al. \(2021\)](#) using their photochemical network and code, and with the sole inclusion of the $\text{O} + \text{H} + \text{H}$ channel the steady-state CH_4 drops from 1% to 3×10^{-5} mixing ratio.

The second reason our results differ has to do with CH_4 production. [Hu et al. \(2021\)](#) modeled Reaction (1d), a critical step to methane formation, with its high-pressure limit rate constant. This approach can accurately estimate the rate at high pressures (~ 100 bar) but substantially over predicts the rate at < 1 bar where third body collisions are more scarce. We have also rerun the 400 ppm- CO_2 model of [Hu et al. \(2021\)](#) using their code, now also with the [Xu et al. \(2015\)](#) pressure-dependent rate constant in Appendix Table A1, and find that the steady-state CH_4 mixing ratio further drops to 2×10^{-7} . This concentration is broadly consistent with model 1 shown in Section 3.1, given remaining subtle differences in the temperature, diffusivity, and radiative transfer.

To further test the above explanation, we have also used the *Photochem* code to reproduce the 400 ppm- CO_2 case in [Hu et al. \(2021\)](#). Adopting their boundary conditions, P-T profile, and eddy diffusion profile, our chemical network predicts 3×10^{-7} mixing ratio CH_4 at steady state. When we perform the same simulation but use the [Hu et al. \(2021\)](#) pressure-independent rate for Reaction (1d), our code predicts 10^{-4} mixing ratio CH_4 should accumulate. When *Photochem* also omits the $\text{O} + \text{H} + \text{H}$ branch of H_2O photolysis, the CH_4 concentration further rises to $\sim 0.5\%$. These *Photochem* results are generally compatible with our [Hu et al. \(2021\)](#) code calculations for the same experiments.

Furthermore, [Madhusudhan et al. \(2023a\)](#) was unable to reproduce [Hu et al. \(2021\)](#) using an independent photochemical model and network. “Case 11” in [Madhusudhan et al. \(2023a\)](#) is very similar to the 10%- CO_2 case in [Hu et al. \(2021\)](#), representing a 1 bar uninhabited Hycean world (i.e., zero-flux boundary conditions for CH_4 and CO). At photochemical steady-state, [Madhusudhan et al. \(2023a\)](#) finds that only 55 ppb CH_4 should persist, which aligns with our conclusion that methane should be a trace gas (e.g., < 1 ppm) on such a planet.

[Yu et al. \(2021\)](#) and [Tsai et al. \(2021a\)](#) also simulated a 1 bar H_2 -dominated atmosphere on K2-18b, but instead with a hot ~ 600 K rocky surface (i.e., no habitable ocean). They find that $\sim 0.1\%$ to 1% CH_4 can accumulate alongside $\sim 1\%$ of CO_2 and CO . We have done similar simulations with the *Photochem* code and found that larger CH_4 concentrations are stable in this case because the hot ~ 600 K surface breaks down the kinetic barriers to CH_4 production. For example,

when temperature is increased from 320 K to 600 K, the rate of the reaction $\text{HCO} + \text{H}_2 \rightarrow \text{H}_2\text{CO} + \text{H}$ increases by about six orders of magnitude while Reaction (2) increases by a factor of ~ 30 . In contrast, methane production is far more kinetically inhibited on a Hycean planet with a habitable 320 K surface (e.g., model 1). Furthermore, the 1 bar scenarios in Yu et al. (2021) and Tsai et al. (2021a) with rocky surfaces can be ruled out because such a planet would be denser than K2-18b’s observed density. To explain the planet’s mass and radius with only a silicate interior and a H_2 -rich envelope, interior modeling suggests the atmosphere needs to be $\gtrsim 1000$ bars thick (Madhusudhan et al. 2020, 2023b).

4.2. Can CH_4 accumulate from non-photochemical abiotic processes?

Substantial methane from non-photochemical abiotic processes is hard to sustain on a Hycean planet. To explain K2-18b’s density, a Hycean world needs a large high-pressure ice layer that separates deep rocky material from the surface water ocean (Madhusudhan et al. 2021). Water-rock reactions and subsequent transport of CH_4 is conceivable (Thompson et al. 2022), but improbable in this case since the high overburden pressure of water and ice inhibits the production of fresh crust to be hydrated (Krissansen-Totton et al. 2021). Moreover, the shutdown of melting of deep-subsurface silicates also precludes the possibility of volcanic CH_4 (Krissansen-Totton et al. 2021; Noack et al. 2016; Kite & Ford 2018). Massive asteroid impacts on the early Earth may have made transient atmospheric methane (Wogan et al. 2023). However, ephemeral impact-induced CH_4 is unlikely on K2-18b because the planet is $\sim 2 - 3$ billion years old (Guinan & Engle 2019), while substantial bombardment is expected to end within the first several hundred million years of planet formation (Lichtenberg & Clement 2022).

4.3. Inhabited Hycean vs. mini-Neptune: evaluating model complexity

Our results suggest that both an inhabited Hycean world (model 2) or a mini-Neptune with a massive H_2 atmosphere (model 3) are not strongly ruled out by the JWST data ($\chi_r^2 \approx 1.5$). However, in addition to evaluating the fit to the data, we also must assess the relative complexity of each scenario. The inhabited Hycean world (model 2) requires a cool habitable surface, but models suggest that a cloud-free 1-bar H_2 -rich atmosphere should trigger a hot runaway greenhouse (Figure 1, Innes et al. 2023; Pierrehumbert 2023). A supercritical steam-dominated atmosphere would have a small scale height incompatible with JWST observations (Scheucher et al. 2020). For a temperate surface, climate codes need to assume the presence of high-altitude clouds or hazes that scatter away starlight (Madhusudhan et al. 2021; Piette & Madhusudhan 2020).

Beyond this climate paradox, ~ 1 bar of H_2 may also be susceptible to rapid escape driven by extreme-ultraviolet radiation (i.e., XUV, Hu et al. 2023). Even if a 1 bar H_2 atmosphere could withstand modern XUV radiation, K2-18b likely experienced exceptionally high XUV fluxes during the host M star’s pre-main sequence, potentially driving hundreds of bars of H_2 loss (Luger et al. 2015), as so a remnant thin ~ 1 bar atmosphere would be highly fortuitous. As noted previously, replenishing H_2 with volcanism would be unlikely on a Hycean K2-18b because rocky material in the deep subsurface would be at pressures too high for melting and outgassing (Kite & Ford 2018; Noack et al. 2016).

In contrast, our model of a gas-giant mini-Neptune (model 3) is relatively straightforward. For a $100\times$ solar composition, solar C/O, and $T_{\text{int}} = 60$ K, which are physically plausible given K2-18b’s mass, a spectrum broadly consistent with the JWST data falls out of our model. Unlike a Hycean world, a mini-Neptune does not require a biosphere to explain the disequilibrium combination of atmospheric CH_4 and CO_2 . Instead, these gases emerge in model 3 from deep-atmosphere quenching (Figure 3). Even though both an inhabited Hycean world and a mini-Neptune are allowed by JWST data, the climate of a Hycean world and the atmosphere’s resilience to escape is hard to explain, so we favor the mini-Neptune model for its simplicity.

While our mini-Neptune simulation is relatively simple, it makes assumptions that should be investigated with more sophisticated modeling. Namely, we simulate the planet’s climate (Figure 3) using a two-stage approach that is not fully self-consistent with photochemistry (Section 2.2), yet an accurate tropopause temperature is important for predicting whether H_2O cold-trapping can reproduce the JWST non-detection of water vapor. The water vapor cold trap would be better approximated by a model that is self-consistent with photochemistry and accounts for the possibility of convection inhibition (Innes et al. 2023). The need for a H_2O cold trap is not unique to a mini-Neptune planet. A Hycean world would also need substantial water condensation to explain the H_2O non-detection. An additional shortcoming of this study is that we only consider one mini-Neptune scenario with a composition of $100\times$ solar metallicity, and solar C/O. Further modeling could tune metallicity and the C/O ratio to get an even better fit to the JWST observations.

4.4. Future observations of K2-18b

Clearly distinguishing between the inhabited Hycean and mini-Neptune interpretations with future JWST observations will be challenging. Ammonia should be unique to a mini-Neptune K2-18b (Figure 3, Yu et al. 2021; Tsai et al. 2021a; Madhusudhan et al. 2023a; Hu et al. 2021). However, even if future observations are unable to detect NH_3 , this would not necessarily prove the inhabited Hycean case. In our mini-Neptune model, the NH_3 features act to fill CH_4 spectral windows (Figure 4). This small ammonia absorption is difficult to distinguish from clouds which have a similar effect on the spectrum (Figure A2). Additionally, there are several reasons why ammonia could be less abundant on a mini-Neptune K2-18b than we have estimated, making a detection even more challenging. Hu (2021) predicted stratospheric NH_3 could be photochemically depleted to undetectable concentrations (< 1 ppm) on a gas-rich K2-18b if tropospheric mixing is slow ($\lesssim 10^3 \text{ cm}^2 \text{ s}^{-1}$). Also, nitrogen could dissolve into a magma ocean at the base of a thick H_2 -rich envelope, preventing a large observable NH_3 abundance in the upper atmosphere (Shorttle et al. 2024).

An inhabited Hycean world could be identified with the detection of a biogenic gas. Madhusudhan et al. (2023b) found weak evidence for dimethyl sulfide (DMS) in K2-18b’s transmission spectrum, a gas almost exclusively produced by life on Earth (Catling et al. 2018). If DMS is detected with statistical significance, it might be difficult to account for its presence without a biosphere on a Hycean planet.

5. CONCLUSIONS

Recent JWST observations of K2-18b (Madhusudhan et al. 2023b), a habitable-zone sub-Neptune exoplanet, revealed the presence of atmospheric CH_4 and CO_2 . Madhusudhan et al. (2023b) suggested that the data are best explained by a habitable “Hycean” world. Our photochemical and climate simulations of K2-18b as a lifeless Hycean world suggest such a planet would have ppb-level CH_4 because the gas is rapidly destroyed by photolysis and subsequent oxidizing reactions. Lacking substantial CH_4 , an uninhabited Hycean planet cannot explain these recent JWST observations, which suggest $\sim 1\%$ of the gas is present (Madhusudhan et al. 2023b). However, there are still two scenarios that fit the JWST observations equally well according to a χ_r^2 metric: a Hycean world inhabited by methanogenic life, or a mini-Neptune with no defined surface. The latter case is less complex and requires fewer assumptions.

Specifically, an inhabited Hycean K2-18b has the following difficulties:

- To explain the $\sim 1\%$ CH_4 detected by JWST, a Hycean planet needs biogenic CH_4 or some other unknown source of the gas to maintain it against photochemical destruction.
- Models predict that a stable temperate climate is challenging on a Hycean K2-18b. Such a planet is expected to experience a steam runaway greenhouse (Figure 1; Innes et al. 2023; Scheucher et al. 2020; Pierrehumbert 2023), unless starlight can be reflected away by clouds (Madhusudhan et al. 2021; Piette & Madhusudhan 2020).
- A thin ~ 1 bar H_2 atmosphere may be susceptible to XUV-driven escape. H_2 can not be replenished by volcanism because the overburden pressure of the thick ice and ocean layer on a Hycean world would prevent silicate melting (Noack et al. 2016; Kite & Ford 2018).

On the other hand, the benefits of the mini-Neptune case are:

- The CH_4 and CO_2 detected by JWST can be broadly explained by deep-atmosphere thermochemical quenching for a $100\times$ solar metallicity, solar C/O, and 60 K intrinsic temperature.
- Deep atmosphere kinetics also predicts NH_3 and CO abundances generally compatible with the JWST non-detections of each gas.
- The lack of H_2O features in the spectrum can be accounted for by water vapor condensation and cold-trapping.
- Basic 1-D radiative-convective-equilibrium modeling can explain the planet’s climate.

Overall, we favor the mini-Neptune explanation of K2-18b because it is simple and has fewer challenges than a Hycean interpretation.

ACKNOWLEDGEMENTS

We thank our anonymous reviewer who improved the quality of this article. Also, we thank Stephen Klippenstein for sharing unpublished reaction rate calculations and improving our understanding of methane kinetics. This work benefited from discussions with Giada Arney, Eddie Schwieterman, Victoria Meadows, Jacob Lustig-Yaeger, Tyler Robinson and Michaela Leung. N.F.W was supported by the NASA Postdoctoral Program. N.E.B acknowledges support from NASA’S Interdisciplinary Consortia for Astrobiology Research (NNH19ZDA001N-ICAR) under award number 19-ICAR19_2-0041. S.-M.T. acknowledges support from NASA Exobiology Grant No. 80NSSC20K1437. R.H. was supported in part by NASA Exoplanets Research Program grant #80NM0018F0612. The research was carried out in part at the Jet Propulsion Laboratory, California Institute of Technology, under a contract with the National Aeronautics and Space Administration.

SOFTWARE

The source code needed to install the necessary software and reproduce all main text calculations (i.e., Figures 1 to 4) is archived on Zenodo: <https://doi.org/10.5281/zenodo.10537133> (Wogan 2024b).

APPENDIX

A. REACTION RATE UPDATES AND THE MINI-NEPTUNE P-T- K_{zz} PROFILE

Table A1 archives the chemical reactions in our network that we updated for this study. Our updated branching ratios for H₂O photolysis are listed in Table A2 based on Slanger & Black (1982) and Stief et al. (1975). Figure A1 illustrates our computed P-T profile for a mini-Neptune K2-18b using the *PICASO* code compared to the modified P-T profile we use in model 3 (see Section 2.2 for details). The figure also shows our assumed K_{zz} profile, which we adopted from Hu (2021).

B. CLOUDS AND HAZES

Here, we consider the effects of clouds and hazes on our K2-18b simulations. In both model 1 and 2, water vapor condenses from the surface to about 0.03 bar forming a cloud deck. Model 3 may also have water vapor clouds caused by condensation between 0.07 bar to 4 mbar. Our photochemical model predicts that hydrocarbon aerosols, similar to Titan’s, are produced in model 2 and 3 at high altitudes (e.g., 10^{-5} bar) because both atmospheres have abundant CH₄. Finally, in model 3, photochemistry processes H₂S to elemental sulfur which condenses to a haze in the same region as the water cloud (Zahnle et al. 2016).

Figure A2 shows simulated spectra of models 1, 2 and 3 that account for these clouds. The calculation uses a range of opacities appropriate for each aerosol. For hydrocarbon aerosols, we adopt real and imaginary indexes of refraction appropriate for a Titan-like haze (Khare et al. 1984). Condensed elemental sulfur has the optical properties shown in Figure S1 of Tian et al. (2010). These indexes of refraction only extend from 0.15 to 0.8 μm , so, following Hu (2021), we constantly extrapolate to longer wavelengths. For both sulfur clouds and hydrocarbon hazes, we use particle densities predicted by the *Photochem* model and assume all aerosols are perfect Mie spheres with a 0.1 μm radius, the size being motivated by the particle radii in Titan’s haze (Rages et al. 1983). Calculations approximate water clouds by simply adding an opaque cloud layer wherever H₂O condenses in the atmosphere.

Overall, our conclusion in the main text that a lifeless Hycean planet (model 1) is ruled out by the JWST data remains unchanged when considering cloudy spectra (Figure A2a). Figure A2b and A2c shows that, like in our clear-sky simulations (Figure 4), the data do not exclude the inhabited Hycean (model 2) or mini-Neptune (model 3) scenarios. Furthermore, the figure reports two χ_r^2 values for each panel: one that includes all the JWST data, and another that excludes the six red data points near 1 μm . This shows that the data scatter near 1 μm has a large effect on the χ_r^2 .

REFERENCES

- Batalha, N., Freedman, R., Gharib-Nezhad, E., & Lupu, R. 2022, Resampled Opacity Database for PICASO, 2.0, Zenodo, doi: [10.5281/zenodo.6928501](https://doi.org/10.5281/zenodo.6928501)
- Batalha, N. E., Marley, M. S., Lewis, N. K., & Fortney, J. J. 2019, ApJ, 878, 70, doi: [10.3847/1538-4357/ab1b51](https://doi.org/10.3847/1538-4357/ab1b51)

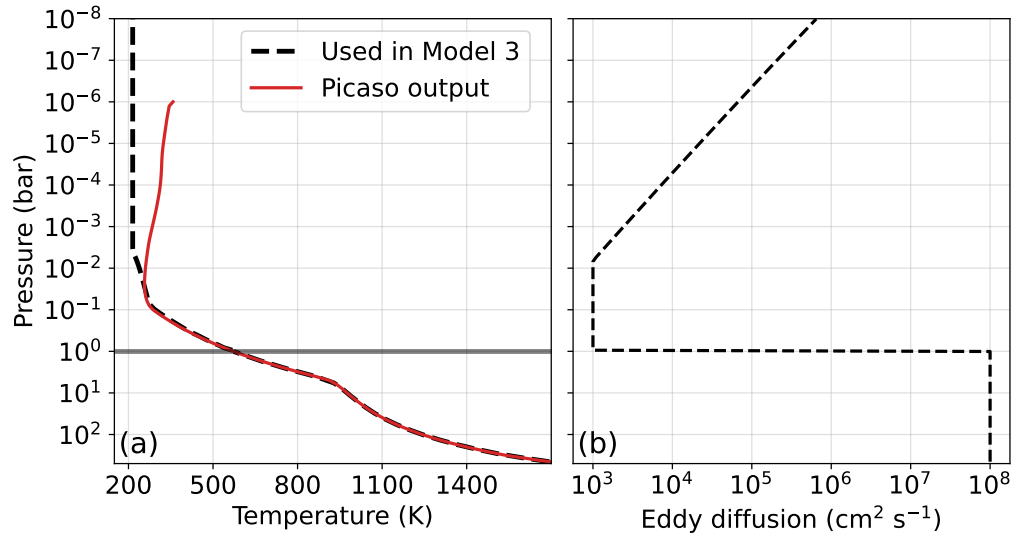


Figure A1. (a) shows the P-T profile for a mini-Neptune K2-18b (model 3). We compute the red P-T profile using the *PICASO* climate model. As described in Section 2.2, we modify the *PICASO* result to make the black dashed P-T profile, which we use in model 3 (Table 1). (b) is the assumed eddy diffusion coefficient for model 3 adopted from Hu (2021).

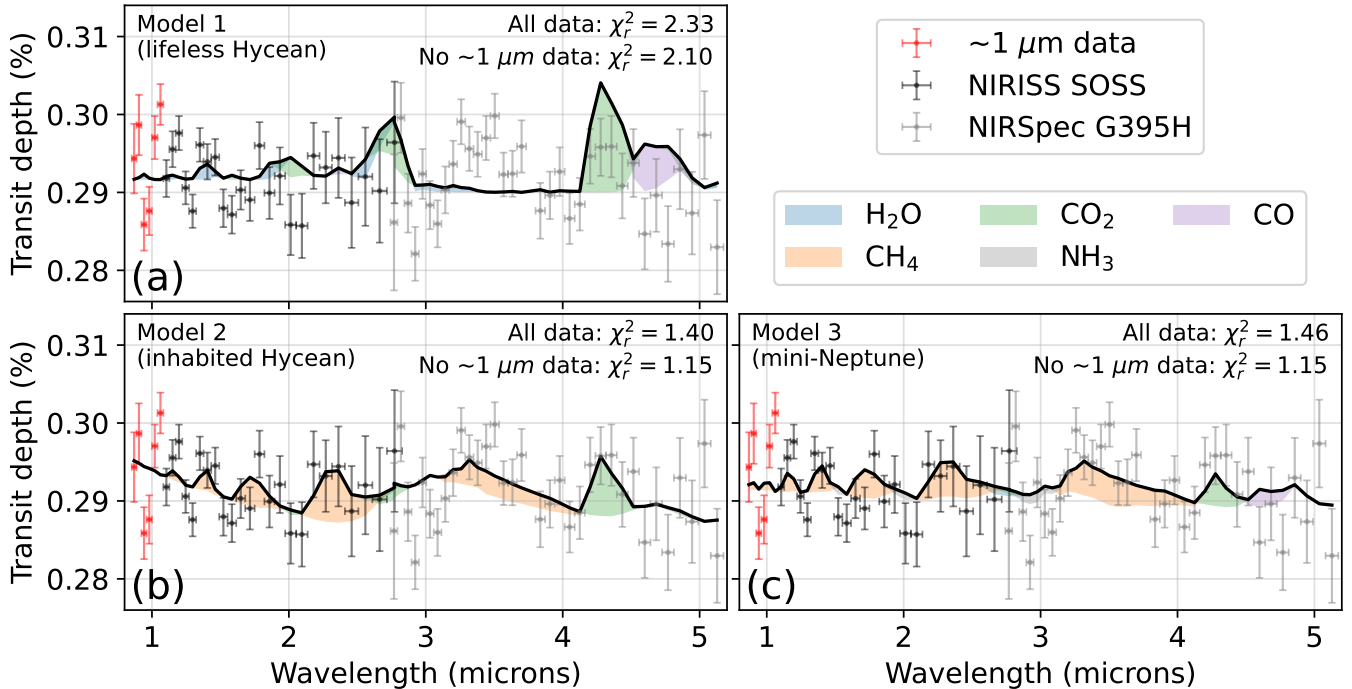


Figure A2. Similar to Figure 4, except all spectral calculations include clouds made of condensed water, elemental sulfur, and hydrocarbons. Each panel reports two χ_r^2 values: one accounts for all the JWST data, while the other excludes the six red points near $1 \mu\text{m}$ to show the effect of this scatter on the χ_r^2 .

Table A1. Updated reaction rates and thermodynamics

Reaction	Rate ^a	Reference
H + H ₂ CO + M → CH ₃ O + M ^b	$k_0 = 1.22 \times 10^{-23} T^{-3} \exp(-2900/T)$ $k_\infty = 6.56 \times 10^3 T^{-5} \exp(-4000/T)$	Xu et al. (2015)
H + H ₂ CO + M → CH ₃ O + M ^b	$k_0 = 9.26 \times 10^{-23} T^{-3.38} \exp(-1432.7/T)$ $k_\infty = 2.65 \times 10^{-2} T^{-3.36} \exp(-2771.4/T)$	Klippenstein (2023)
H + H ₂ CO + M → H ₂ COH + M ^b	$k_0 = 2.82 \times 10^{-29} T^{-1.2} \exp(-2900/T)$ $k_\infty = 3 \times 10^{-12} \exp(-3500/T)$	Xu et al. (2015)
H + H ₂ CO + M → H ₂ COH + M ^b	$k_0 = 2.99 \times 10^{-21} T^{-3.4} \exp(-2127.5/T)$ $k_\infty = 1.92 \times 10^{-25} T^{3.89} \exp(-516.9/T)$	Klippenstein (2023)
CH ₃ + O → H ₂ CO + H	9×10^{-11}	Xu et al. (2015)
CH ₃ + O → HCO + H ₂	6×10^{-11}	Xu et al. (2015)
H ₂ CO + H → HCO + H ₂	$2.28 \times 10^{-19} T^{2.65} \exp(-766.5/T)$	Xu et al. (2015)
H ₂ O + $h\nu$ → OH + H	Determined by photolysis cross section ^c	Slanger & Black (1982); Stief et al. (1975)
H ₂ O + $h\nu$ → H ₂ + O(¹ D)	Determined by photolysis cross section ^c	Slanger & Black (1982); Stief et al. (1975)
H ₂ O + $h\nu$ → O + H + H	Determined by photolysis cross section ^c	Slanger & Black (1982); Stief et al. (1975)
H ₂ + $h\nu$ → H + H	Determined by photolysis cross section	Heays et al. (2017)
Species	Enthalpy ^d (KJ/mol)	Reference
CH ₃ O	21.6	Xu et al. (2015)
H ₂ COH	-15.3	Xu et al. (2015)

^aLow pressure rate constants, k_0 , have units $\text{cm}^6 \text{ molecules}^{-2} \text{ s}^{-1}$. All other rates have units $\text{cm}^3 \text{ molecules}^{-1} \text{ s}^{-1}$.

^bReactions H + H₂CO + M → CH₃O + M and H + H₂CO + M → H₂COH + M have two rate entries. We nominally adopt the rate from Xu et al. (2015) but also consider the Klippenstein (2023) rate as a sensitivity test (Section 3.1).

^cWe updated the branching ratios for these three reactions, but not the total photolysis cross section.

^dEnthalpy of formation at 298 K.

Table A2. Updated H₂O photolysis branching ratios

Wavelength ^a (nm)	OH + H	H ₂ + O(¹ D)	O + H + H
92.5	0.89	0.11	0
120.9	0.89	0.11	0
121.0	0.78	0.1	0.12
122.1	0.89	0.11	0
145.0	1	0	0
251.6	1	0	0

^aBranching ratios are linearly interpolate to intermediate wavelengths.

- Benneke, B., Wong, I., Piaulet, C., et al. 2019, *ApJL*, 887, L14, doi: [10.3847/2041-8213/ab59dc](https://doi.org/10.3847/2041-8213/ab59dc)
- Catling, D. C., Krissansen-Totton, J., Kiang, N. Y., et al. 2018, *Astrobiology*, 18, 709, doi: [10.1089/ast.2017.1737](https://doi.org/10.1089/ast.2017.1737)
- Fortney, J. J., Visscher, C., Marley, M. S., et al. 2020, *AJ*, 160, 288, doi: [10.3847/1538-3881/abc5bd](https://doi.org/10.3847/1538-3881/abc5bd)
- France, K., Loyd, R. O. P., Youngblood, A., et al. 2016, *ApJ*, 820, 89, doi: [10.3847/0004-637X/820/2/89](https://doi.org/10.3847/0004-637X/820/2/89)
- Fulton, B. J., & Petigura, E. A. 2018, *AJ*, 156, 264, doi: [10.3847/1538-3881/aae828](https://doi.org/10.3847/1538-3881/aae828)
- Graham, R. J., Lichtenberg, T., Boukrouche, R., & Pierrehumbert, R. T. 2021, *PSJ*, 2, 207, doi: [10.3847/PSJ/ac214c](https://doi.org/10.3847/PSJ/ac214c)
- Guinan, E. F., & Engle, S. G. 2019, *Research Notes of the American Astronomical Society*, 3, 189, doi: [10.3847/2515-5172/ab6086](https://doi.org/10.3847/2515-5172/ab6086)
- Heays, A. N., Bosman, A. D., & van Dishoeck, E. F. 2017, *A&A*, 602, A105, doi: [10.1051/0004-6361/201628742](https://doi.org/10.1051/0004-6361/201628742)
- Hu, R. 2021, *ApJ*, 921, 27, doi: [10.3847/1538-4357/ac1789](https://doi.org/10.3847/1538-4357/ac1789)
- Hu, R., Damiano, M., Scheucher, M., et al. 2021, *ApJL*, 921, L8, doi: [10.3847/2041-8213/ac1f92](https://doi.org/10.3847/2041-8213/ac1f92)
- Hu, R., Gaillard, F., & Kite, E. S. 2023, *ApJL*, 948, L20, doi: [10.3847/2041-8213/acd0b4](https://doi.org/10.3847/2041-8213/acd0b4)
- Innes, H., Tsai, S.-M., & Pierrehumbert, R. T. 2023, *ApJ*, 953, 168, doi: [10.3847/1538-4357/ace346](https://doi.org/10.3847/1538-4357/ace346)
- Jackson, R. B., Saunio, M., Bousquet, P., et al. 2020, *Environmental Research Letters*, 15, 071002, doi: [10.1088/1748-9326/ab9ed2](https://doi.org/10.1088/1748-9326/ab9ed2)
- Khare, B. N., Sagan, C., Arakawa, E. T., et al. 1984, *Icarus*, 60, 127, doi: [10.1016/0019-1035\(84\)90142-8](https://doi.org/10.1016/0019-1035(84)90142-8)
- Kharecha, P., Kasting, J., & Siefert, J. 2005, *Geobiology*, 3, 53, doi: [10.1111/j.1472-4669.2005.00049.x](https://doi.org/10.1111/j.1472-4669.2005.00049.x)
- Kite, E. S., & Ford, E. B. 2018, *ApJ*, 864, 75, doi: [10.3847/1538-4357/aad6e0](https://doi.org/10.3847/1538-4357/aad6e0)
- Klippenstein, S. J. 2023, Private Communication
- Krissansen-Totton, J., Galloway, M. L., Wogan, N., Dhaliwal, J. K., & Fortney, J. J. 2021, *ApJ*, 913, 107, doi: [10.3847/1538-4357/abf560](https://doi.org/10.3847/1538-4357/abf560)
- Lichtenberg, T., & Clement, M. S. 2022, *ApJL*, 938, L3, doi: [10.3847/2041-8213/ac9521](https://doi.org/10.3847/2041-8213/ac9521)
- Luger, R., Barnes, R., Lopez, E., et al. 2015, *Astrobiology*, 15, 57, doi: [10.1089/ast.2014.1215](https://doi.org/10.1089/ast.2014.1215)
- Madhusudhan, N., Moses, J. I., Rigby, F., & Barrier, E. 2023a, *Faraday Discussions*, 245, 80, doi: [10.1039/D3FD00075C](https://doi.org/10.1039/D3FD00075C)
- Madhusudhan, N., Nixon, M. C., Welbanks, L., Piette, A. A., & Booth, R. A. 2020, *ApJL*, 891, L7, doi: [10.3847/2041-8213/ab7229](https://doi.org/10.3847/2041-8213/ab7229)
- Madhusudhan, N., Piette, A. A. A., & Constantinou, S. 2021, *ApJ*, 918, 1, doi: [10.3847/1538-4357/abfd9c](https://doi.org/10.3847/1538-4357/abfd9c)
- Madhusudhan, N., Sarkar, S., Constantinou, S., et al. 2023b, *ApJL*, 956, L13, doi: [10.3847/2041-8213/acf577](https://doi.org/10.3847/2041-8213/acf577)
- Mollière, P., Wardenier, J. P., van Boekel, R., et al. 2019, *A&A*, 627, A67, doi: [10.1051/0004-6361/201935470](https://doi.org/10.1051/0004-6361/201935470)
- Moses, J. I., Bézard, B., Lellouch, E., et al. 2000, *Icarus*, 143, 244, doi: [10.1006/icar.1999.6270](https://doi.org/10.1006/icar.1999.6270)
- Mukherjee, S., Batalha, N. E., Fortney, J. J., & Marley, M. S. 2023, *ApJ*, 942, 71, doi: [10.3847/1538-4357/ac9f48](https://doi.org/10.3847/1538-4357/ac9f48)
- Noack, L., Höning, D., Rivoldini, A., et al. 2016, *Icarus*, 277, 215, doi: [10.1016/j.icarus.2016.05.009](https://doi.org/10.1016/j.icarus.2016.05.009)
- Pierrehumbert, R. T. 2023, *ApJ*, 944, 20, doi: [10.3847/1538-4357/acafdf](https://doi.org/10.3847/1538-4357/acafdf)
- Piette, A. A. A., & Madhusudhan, N. 2020, *ApJ*, 904, 154, doi: [10.3847/1538-4357/abfbf1](https://doi.org/10.3847/1538-4357/abfbf1)
- Rages, K., Pollack, J. B., & Smith, P. H. 1983, *J. Geophys. Res.*, 88, 8721, doi: [10.1029/JA088iA11p08721](https://doi.org/10.1029/JA088iA11p08721)
- Scheucher, M., Wunderlich, F., Grenfell, J. L., et al. 2020, *ApJ*, 898, 44, doi: [10.3847/1538-4357/ab9084](https://doi.org/10.3847/1538-4357/ab9084)
- Shorttle, O., Jordan, S., Nicholls, H., Lichtenberg, T., & Bower, D. J. 2024, arXiv e-prints, arXiv:2401.05864, doi: [10.48550/arXiv.2401.05864](https://doi.org/10.48550/arXiv.2401.05864)
- Slanger, T. G., & Black, G. 1982, *JChPh*, 77, 2432, doi: [10.1063/1.444111](https://doi.org/10.1063/1.444111)
- Stief, L. J., Payne, W. A., & Klemm, R. B. 1975, *JChPh*, 62, 4000, doi: [10.1063/1.430323](https://doi.org/10.1063/1.430323)
- Thompson, M. A., Krissansen-Totton, J., Wogan, N., Telus, M., & Fortney, J. J. 2022, *Proceedings of the National Academy of Science*, 119, e2117933119, doi: [10.1073/pnas.2117933119](https://doi.org/10.1073/pnas.2117933119)
- Tian, F., Claire, M. W., Haqq-Misra, J. D., et al. 2010, *Earth and Planetary Science Letters*, 295, 412, doi: [10.1016/j.epsl.2010.04.016](https://doi.org/10.1016/j.epsl.2010.04.016)
- Tsai, S.-M., Innes, H., Lichtenberg, T., et al. 2021a, *ApJL*, 922, L27, doi: [10.3847/2041-8213/ac399a](https://doi.org/10.3847/2041-8213/ac399a)
- Tsai, S.-M., Malik, M., Kitzmann, D., et al. 2021b, *ApJ*, 923, 264, doi: [10.3847/1538-4357/ac29bc](https://doi.org/10.3847/1538-4357/ac29bc)
- Wogan, N. 2024a, photochem, v0.4.5, Zenodo, doi: [10.5281/zenodo.10524976](https://doi.org/10.5281/zenodo.10524976)
- . 2024b, Code for reproducing K2-18b article, v1.0.1, Zenodo, doi: [10.5281/zenodo.10537133](https://doi.org/10.5281/zenodo.10537133)
- Wogan, N. F., & Catling, D. C. 2020, *ApJ*, 892, 127, doi: [10.3847/1538-4357/ab7b81](https://doi.org/10.3847/1538-4357/ab7b81)
- Wogan, N. F., Catling, D. C., Zahnle, K. J., & Lupu, R. 2023, *PSJ*, 4, 169, doi: [10.3847/PSJ/aced83](https://doi.org/10.3847/PSJ/aced83)
- Xu, Z. F., Raghunath, P., & Lin, M. C. 2015, *Journal of Physical Chemistry A*, 119, 7404, doi: [10.1021/acs.jpca.5b00553](https://doi.org/10.1021/acs.jpca.5b00553)
- Yu, X., Moses, J. I., Fortney, J. J., & Zhang, X. 2021, *ApJ*, 914, 38, doi: [10.3847/1538-4357/abfd9c](https://doi.org/10.3847/1538-4357/abfd9c)

Zahnle, K., Marley, M. S., Morley, C. V., & Moses, J. I.
2016, *ApJ*, 824, 137, doi: [10.3847/0004-637X/824/2/137](https://doi.org/10.3847/0004-637X/824/2/137)